GSI

GSI-93-54
PREPRINT
JULI 1993

BREAKUP CONFIGURATIONS IN MULTIPLE DISINTEGRATION OF PROJECTILE FRAGMENTS

V. LINDENSTRUTH et al.

Gesellschaft für Schwerionenforschung mbH
Postfach 110552 · D-64220 Darmstadt · Germany

Breakup Configurations in Multiple Disintegration of Projectile Fragments

V. Lindenstruth,[1] J. Pochodzalla,[1] J.C. Adloff,[3] M. Begemann-Blaich,[1] P. Bouissou,[4] J. Hubele,[1] G. Imme,[5] I. Iori,[6] P. Kreutz,[2] G.J. Kunde,[1] S. Leray,[4] Z. Liu,[1] U. Lynen,[1] R.J. Meijer,[1] U. Milkau,[1] A. Moroni,[6] W.F.J. Müller,[1] C. Ngô,[4] C.A. Ogilvie,[1] G. Raciti,[5] G. Rudolf,[3] H. Sann,[1] A. Schüttauf,[2] W. Seidel,[7] L. Stuttge,[3] W. Trautmann,[1] and A. Tucholski[1]

[1]*Gesellschaft für Schwerionenforschung, D-64220 Darmstadt, Germany*

[2]*Institut für Kernphysik, Universität Frankfurt, D-60486 Frankfurt, Germany*

[3]*Centre de Recherches Nucléaires, F-67037 Strasbourg, France*

[4]*Laboratoire National Saturne, CEN Saclay, F-91191 Gif-sur-Yvette, France*

[5]*Dipartimento di Fisica dell' Universitá and I.N.F.N., I-95129 Catania, Italy*

[6]*Instituto di Scienze Fisiche, Universita degli Studi di Milano and I.N.F.N., I-20133 Milano, Italy*

[7]*Forschungszentrum Rossendorf, Postfach 510119, D-01314 Dresden, Germany*

ABSTRACT

Kinematic correlations between three heavy projectile fragments produced in Au induced reactions at E/A = 600 MeV are presented. The sensitivity of these correlations to the disassembly geometry is confirmed by classical three-body trajectory calculations. The simulations suggest a fast disintegration process of an highly excited system. Within the assumed scenarios the data constrain a possibly existing radial flow to a maximum value of about 1 MeV per nucleon. This radial motion can be provided by the Coulomb repulsion between the fragments if the breakup occurs out of a volume with a radius not larger than 15 fm.

PACS numbers: 24.60.Ky, 25.40.Sc, 25.70.Np

In several recent experiments indirect evidence for a fast breakup of excited nuclear systems has been accumulated by comparing measured fragment yields with predictions based on statistical decay models [1, 2, 3]. Nonetheless, a definite picture of the multifragmentation dynamics has not yet emerged. Besides multisequential binary decays at low nuclear densities [4], condensation processes in an expanded nuclear system – which may provide a link to a nuclear liquid-gas phase transition [5, 6] – have been discussed as a conceivable scenario [7, 8, 9]. More recently, shape instabilities as a consequence of surface fluctuations have been proposed [10, 11] as a trigger for the fragmentation process.

Observable and characteristic fingerprints of the disintegration dynamics may show up in kinematic correlations which are governed by the long-range Coulomb repulsion [12-20]. First studies of fragment-fragment proximity correlations at intermediate energies 20 MeV $\leq$ E/A $\leq$ 100 MeV suggested emission times which were consistent with a sequential decay process [14, 16]. Using heavier projectiles, Kim and co-workers deduced a rather short emission time for light fragments produced in central ^{36}Ar + ^{197}Au collisions at E/A = 35 MeV [17, 18]. However, the dominance of preequilibrium processes in these reactions [14, 18, 21] renders a clean separation between different sources of fragments to be difficult. Furthermore, in most two-fragment correlation studies no information about possibly existing heavy target remnants [14, 19] is available thus leading to uncertainties of the extracted emission times because of the unknown recoil effects [22] and because of velocity fluctuations of the emitting system. Indeed, Bizard and co-workers showed in a more complete study that the relative velocity distributions of three coincident heavy fragments produced in the similar reaction ^{40}Ar + ^{197}Au at E/A = 30 MeV are consistent with a sequential production mechanism [19]. In line with this study in the Fermi energy domain we present in this letter kinematic correlations between three heavy projectile fragments produced in Au induced relativistic heavy ion collisions.

The experiment was performed with the ALADIN spectrometer at SIS [23, 24]. Targets of C, Al, Cu and Pb with about 3 % interaction probability were bombarded with a Au beam with an energy of 600 MeV per nucleon. Heavy fragments with charge $Z \geq 8$ were identified according to their atomic number and tracked by a multiple-sampling ionization chamber (TP-MUSIC) [25]. The charge of all other light fragments with $2 \leq Z \leq 7$ was determined by a plastic scintillator wall. This array also provided the time-of-flight (TOF) for all projectile fragments with $Z \geq 2$. Combining the TOF and the TP-MUSIC information, the mass of fragments with $Z \geq 8$ was evaluated with a relative resolution of $\Delta A/A \approx 3\%$ (FWHM) .

We will consider only those events where exactly three fragments were tracked in the TP-MUSIC. For this event class Z_{bound}, defined as the summed charge of all projectile fragments with $Z \geq 2$ [23], varies between 45 and 70 and peaks at $Z_{bound} \approx 55$. Typically 80 % of Z_{bound} is contained in the charges of the three heaviest fragments. Sorted according to their charge number, the average charges and masses of these fragments i=1-3 are $\langle Z_i \rangle$ = 22, 13, 10 and $\langle A_i \rangle$ = 48, 29, 20.

The momenta of the fragments are expected to reflect the breakup dynamics. In the present analysis the momenta $\vec{p}_{c.m.,i}$ of the three fragments in their center-of-momentum (c.m.) frame are used to determine the summed c.m. - kinetic energy

$$E_3 = \sum_{i=1}^{3} p^2_{c.m.,i}/(2 \cdot m_0 \cdot A_i) \qquad (1)$$

where m_0 is the atomic mass unit. In Figure 1 the average value $\langle E_3 \rangle$ (top part) and the standard deviation σ_3 of E_3 (bottom part) are displayed as a function of the sum of a nominal Coulomb repulsion

$$E_c = e^2 \cdot \sum_{i<j} Z_i Z_j/(r_0(A_i^{1/3} + A_j^{1/3})). \qquad (2)$$

For the radius parameter r_0 a value of 1.4 fm was used in all calculations. Within the statistical uncertainties no target dependence is apparent and the data depend

linearly on E_c. We, therefore, parameterized our observations in terms of two straight line fits common to the data points of all targets. The slope and intercept of these fits are $m_E = 0.37 \pm 0.04$ and $b_E = 76 \pm 5$ MeV for $\langle E_3 \rangle$ and m_σ = -0.07 $\pm$ 0.01 and $b_\sigma = 44 \pm 4$ MeV for σ_3.

Although significant progress in the development of microscopic transport models has been achieved during the last decade [26], a detailed and consistent microscopic theory which describes both, the disassembly dynamics as well as the formation of *observable* fragments is not yet available. In order to test the sensitivity of our observations to the breakup geometry we, therefore, performed classical three-body trajectory calculations. We examine two schematic disintegration configurations which mimic the main categories of breakup scenarios discussed in the literature [1, 2, 3]:
(i) The first class simulates two sequential, binary splittings of the initial nucleus. In both steps, the surfaces of the two produced fragments were initially separated by a fixed distance 2·D. The time delay t between the two decays was chosen from an exponential distribution $P(t) \propto exp(-ln2 \cdot t/\tau)$. The initial relative energy of the two fragments was selected from a distribution

$$P(E) \propto E^\alpha \cdot exp(-E/T) \tag{3}$$

where for the exponent α values of 0.5 or 1 were used. The direction of the corresponding initial relative velocity was isotropically [27] distributed.
(ii) With the second type of simulations a simultaneous emission out of a given volume is modelled. The centers of the three non-overlapping fragments are distributed randomly within a sphere of radius R. To each fragment an isotropically distributed initial velocity was assigned. Constrained by total momentum conservation, these velocities were selected according to the energy distribution described by Eq. 3. In addition to this random motion, an initial radial flow velocity $\vec{v}_{f,i} = (2\epsilon_f/m_0)^{1/2} \cdot \vec{d}_i/R$ was taken into account. Here, $\vec{d}_i$ is the position of the center of the fragment i with respect to the center-of-momentum, and the parameter ϵ_f denotes the flow energy per

nucleon for fragments located at d_i = R.

The charges and masses of the fragments were obtained by a Monte Carlo sampling of the measured events, thus reducing significantly the uncertainties associated with the fragment distribution. For each event the temperature parameter T was chosen according to the experimental value of Z_{bound} from the relation $T = f_T \cdot (2 \cdot (79 - Z_{bound}))^{1/2}$, where f_T is a free parameter. For $f_T = 1$ this relation describes within the relevant range of Z_{bound} the temperatures of the initial projectile spectators as predicted by microscopic transport calculations [3] reasonably well. The paths of the fragments were calculated under the influence of their mutual Coulomb field and two-fragment proximity forces according to Ref. [28]. Since for the further analysis those trajectories were rejected for which the fragments did overlap during the propagation, the influence of the proximity force turns out to be rather small. In order to account for the recoil from light particles emitted sequentially from the initial fragments, the measured charges and masses were increased prior to the trajectory calculations in accordance with the initial temperature. After the fragment-fragment interaction has ceased, the sequential emission of light particles leading to the observed masses and charges was assumed to take place.

In order to quantify the agreement between the simulations and the experimental observations we define a reduced χ^2

$$\chi^2 = \frac{1}{5} \sum_{i=1}^{5} (x_i - y_i)^2 / \delta_i^2 \ . \tag{4}$$

Here, x_i are the four coefficients characterizing the fits to the data in Fig. 1 and, in addition, the mean scaled [17] relative velocity between the two lighter fragments 2 and 3, $\langle \beta_{23} / \sqrt{Z_2 + Z_3} \rangle = 0.0206 \pm 0.0005$. δ_i and y_i denote the experimental uncertainties of these quantities and the corresponding model predictions, respectively [29].

The results of the sequential type of calculations are summarized in Fig. 2. The box-plot in part (a) displays for a given lifetime of τ = 100 fm/c the variation of χ^2 as a

function of the two other model parameters f_T and D. For orientation, contour lines for $\chi^2 = 4$ and 10 are shown. A distinct minimum at D = 2 ± 0.5 fm and $f_T = 1.25 \pm 0.05$ can be discerned. Within the quoted uncertainties, similar minima were found at the *same* values of D and f_T for all considered values of $\tau \leq 10^4 fm/c$. However, the height of this minimum, χ^2_{min}, increases strongly for large values of τ (Fig. 2b) and clearly excludes emission times $\tau > 2000$ fm/c. The good agreement of the simulations with the data for smaller values of τ is illustrated in parts c and d of Fig. 2 [30]. Whereas the E_c dependences of $\langle E_3 \rangle$ and σ_3 provide no further constraint on τ, the probability distribution P_{23} of β_{23} is best reproduced by calculations using small $\tau \sim 10$ fm/c (solid line in Fig. 2e). This preference for very small relative emission times is even more evident in Fig. 2f where we compare the measured and predicted correlation functions [14] of fragment 2 and 3, $R_{23}(\beta_{23})+1$. Note that the background events for the correlation functions were generated by using the c.m. momenta, thus minimizing the uncertainty associated with the collective velocity of the decaying system.

Results of calculations modelling the simultaneous volume emission of the three fragments are compiled in Fig. 3. Similar to the case of the sequential simulations a clear minimum of χ^2 can be determined for each given flow parameter ϵ_f by varying independently the other two model parameters R and f_T. Part a of Fig. 3 shows in a R - f_T plane the contour lines with $\chi^2 = 2$ for $\epsilon_f = 0$ (at R ≈ 15 fm), 0.5 (R ≈ 22 fm) and 1 MeV (R ≈ 26 fm) and for two different values for the exponent α. The corresponding minimal χ^2 are displayed in part b as a function of ϵ_f. Values of ϵ_f larger than 1 MeV are ruled out whereas smaller values of ϵ_f show no significantly different χ^2_{min}. Nonetheless, for each given value of α there exists a rather unique relation between ϵ_f, R and f_T. For large emission radii R the data can only be described if a collective radial velocity is taken into account. This radial motion can be provided by the Coulomb repulsion between the fragments if the breakup occurs out of a volume with R = 15 fm. The corresponding average initial distance between fragment 2 and

3 is about $\langle d_{23} \rangle \approx 18$ fm and is comparable to a value of $\langle d_{23} \rangle \approx 16$ fm obtained for the sequential scenario using $\tau = 10$ fm/c.

The interplay between the Coulomb repulsion on one hand and the initial velocity - composed of the random thermal motion and the radial flow - on the other hand, is exemplified in Fig. 3c and d. Adopting the optimal parameter set for the case ϵ_f = 0.5 MeV and $\alpha = 1$, i.e. R=22.5 fm and $f_T = 1.2$, the sequential evaporation (E), flow (F) and the Coulomb repulsion (C) have been added successively to the initial thermal energy (T). The decrease of the thermal contribution by about 5 MeV when going from $\epsilon_f = 0$ (f_T= 1.35) to $\epsilon_f = 0.5$ MeV (f_T=1.2) is small compared to the additional contribution of 20 MeV which is due to the radial flow. Furthermore, the dotted histogram in Fig. 3c illustrates that the slope parameter m_E is also affected by the increasing temperature in more central collisions which are characterized by smaller average fragment charges and hence smaller values of E_c. Finally, we show in panels e and f of Fig. 3 that also for this emission geometry, the relative velocity distribution of fragment 2 and 3 and the correlation function $R_{23} + 1$ are reasonably well reproduced for all values of $\epsilon_f \leq 1$ MeV [30].

In conclusion, we have studied kinematic correlations between three heavy projectile fragments produced in Au induced reactions at E/A = 600 MeV. A comparison of the observed correlations to schematic trajectory calculations indicates a strong sensitivity to the disassembly geometry. Although the present data do not allow to unequivocally determine this geometry, they significantly limit the possible parameter space of the breakup scenario. The simulations suggest a fast disintegration process of an highly excited and rather extended nuclear system. Because of the stronger Coulomb repulsion, smaller emission volumes would require lower temperature parameters leading to smaller fluctuations of the kinetic energies. Although we can not exclude that the resulting underprediction of σ_3 may be compensated by fluctuations of the initial excitation energy, the observed sensitivities raise the hope, that these data

will not only narrow the parameter space for such extended parametrizations or other conceivable fragmentation scenarios [10, 11] but also for more specific disintegration models [8, 9].

This work was partly supported by the Bundesministerium für Forschung und Technologie. One of us (J.P.) acknowledges the financial support of the Deutsche Forschungsgemeinschaft.

References

[1] D.R. Bowman *et al.*, Phys. Rev. Lett. **67**, 1527 (1991).

[2] K. Hagel *et al.*, Phys. Rev. Lett. **68**, 2141 (1992).

[3] J. Hubele *et al.*, Phys. Rev. C **46**, R1577 (1992).

[4] W.A. Friedman, Phys. Rev. C **42**, 667 (1990).

[5] P.J. Siemens, Nature (London) **305**, 410 (1983).

[6] G.F. Bertsch and P.J. Siemens, Phys. Lett. B **126B**, 9 (1983).

[7] A.S. Botvina, A.S. Il'inov, and I.N. Mishustin, Yad. Fiz. **42**, 1127 (1985) [Sov. J. Nucl. Phys. **42**, 712 (1985)].

[8] J. Bondorf *et al.*, Nucl. Phys. **A443**, 321 (1985).

[9] D.H.E. Gross *et al.*, Phys. Rev. Lett. **56**, 1544 (1986).

[10] L.G. Moretto *et al.*, Phys. Rev. Lett. **69**, 1884 (1992).

[11] W. Bauer, G.F. Bertsch, and H. Schulz, Phys. Rev. Lett. **69**, 1888 (1992).

[12] P. Glässel *et al.*, Z. Phys. A - Atoms and Nuclei **310**, 189 (1983).

[13] D. Pelte *et al.*, Phys. Rev. C **34**, 1673 (1986).

[14] R. Trockel *et al.*, Phys. Rev. Lett. **59**, 2844 (1987).

[15] D.H.E. Gross *et al.*, Phys. Lett. B **224**, 29 (1989).

[16] R. Bougault *et al.*, Phys. Lett. B **232**, 291 (1989).

[17] Y.D. Kim *et al.*, Phys. Rev. Lett. **67**, 14 (1991).

[18] Y.D. Kim *et al.*, Phys. Rev. C 45, 338 (1992)

[19] G. Bizard *et al.*, Phys. Lett. B 276, 413 (1992).

[20] D.R. Bowman *et al.*, Phys. Rev. Lett. 70, 3534 (1993).

[21] J.L. Wile *et al.*, Phys. Rev. C 45, 2300 (1992).

[22] J. Pochodzalla *et al.*, Phys. Lett. B 232, 41 (1989)

[23] J. Hubele *et al.*, Z. Phys. A 340, 263 (1991).

[24] P. Kreutz *et al.*, Nucl. Phys. A (in print)

[25] W.B. Christie *et al.*, Nucl. Instr. and Meth. in Phys. Res. A255, 466 (1987).

[26] See e.g. in *The Nuclear Equation of State, Part A and B*, Edt. W. Greiner and H. Stöcker, Plenum Press, New York.

[27] We have verified that the normal vector of the plane which is spanned by the momenta of the three fragments is isotropically distributed in space. This signals a small angular momentum transfer and/or a large angular momentum misalignment and is consistent with an isotropic breakup.

[28] J. Lopez and J. Randrup, Nucl. Phys. A503, 183 (1989).

[29] Calculations which did not include $\langle\beta_{23}\rangle$ in the χ^2 - determination gave within the quoted uncertainties the same optimal temperature scaling factors f_T but up to 20% larger distances between the centers of the fragments for a given flow ϵ_f or lifetime τ.

[30] We have checked that with these optimal parameter sets also the single particle c.m.-observables were reproduced at the same level of accuracy.

Figure 1:

Mean center-of-mass total kinetic energy $\langle E_3 \rangle$ (top) and the standard deviation σ_3 (bottom) as a function of the nominal Coulomb energy for the three largest projectile fragments emitted in Au + C, Al, Cu and Pb collisions at E/A = 600 MeV. The points were obtained by sorting the data in 30 MeV wide bins.

Figure 2:

Summary of the sequential decay calculations. Part a: Two-dimensional display of χ^2 as a function of the initial fragment-fragment separation D and the scaling factor f_T of the temperature for a life time τ = 100 fm/c. The area of the largest box corresponds to $\chi^2 = 50$. Part b: Minimum χ^2 as a function of the lifetime τ. Parts c and d: Optimal predictions for $\langle E_3 \rangle$ and σ_3 for different lifetimes τ. Parts e and f: Coincidence yield and two-fragment correlation function of fragment 2 and 3 as a function of their scaled relative velocity for the optimum parameter set with D=2 fm and $f_T = 1.25$ and the indicated values of τ.

Figure 3:

Summary of calculations assuming a volume emission. Part a: Contour lines for χ^2 in a plane defined by the volume radius R and the scaling factor f_T of the temperature for flow parameters ϵ_f = 0, 0.5 and 1 MeV (increasing from left to right). Part b: Minimum χ^2 as a function of ϵ_f. Parts c and d: Predictions for $\langle E_3 \rangle$ and σ_3 for the case $\epsilon_f = 0.5$ MeV. Parts e and f: Coincidence yields and two-fragment correlation function of fragment 2 and 3 as a function of their scaled relative velocity adopting the optimum parameter set for the indicated flow energy.

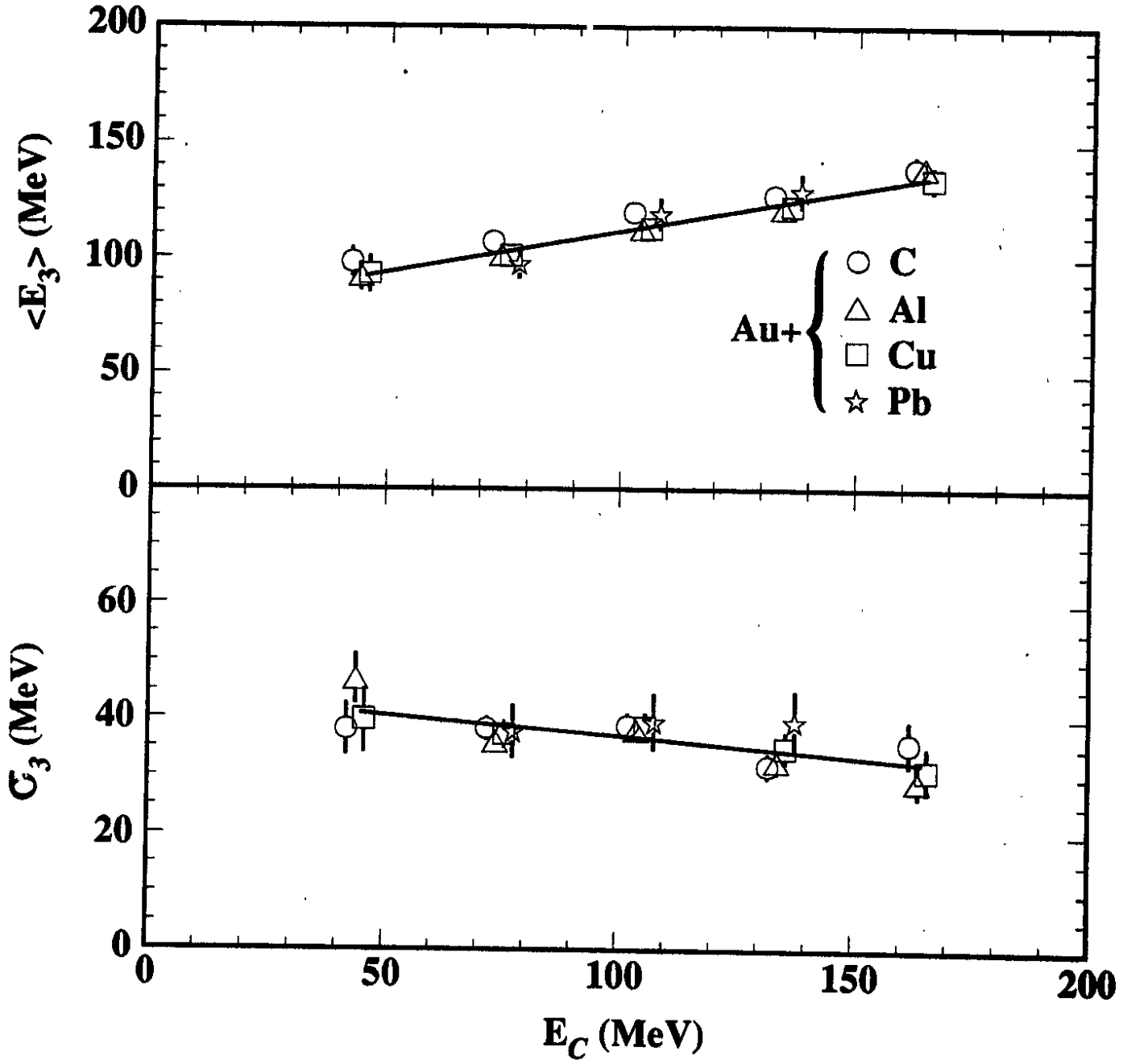
200
150
100
50
0
<E3> (MeV)
Au+
C
Al
Cu
Pb
60
40
20
0
σ3 (MeV)
0
50
100
150
200
EC (MeV)

Figure 1:

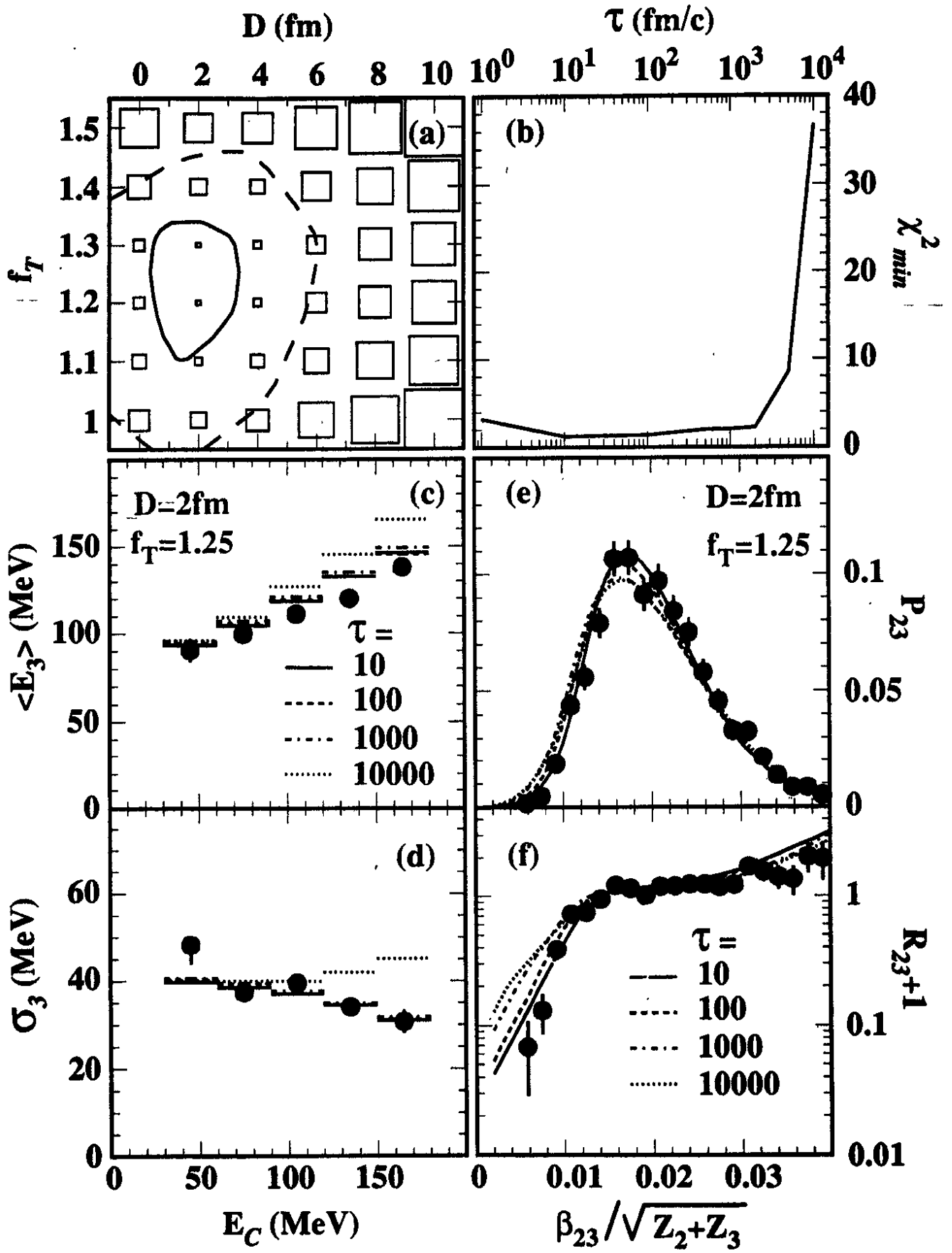
D (fm)
τ (fm/c)
(a)
(b)
(c)
(d)
(e)
(f)
D=2fm
f_T=1.25
τ =
10
100
1000
10000
f_T
χ²_min
<E_3> (MeV)
σ_3 (MeV)
P_23
R_23+1
E_C (MeV)
β_23/√(Z_2+Z_3)

Figure 2:

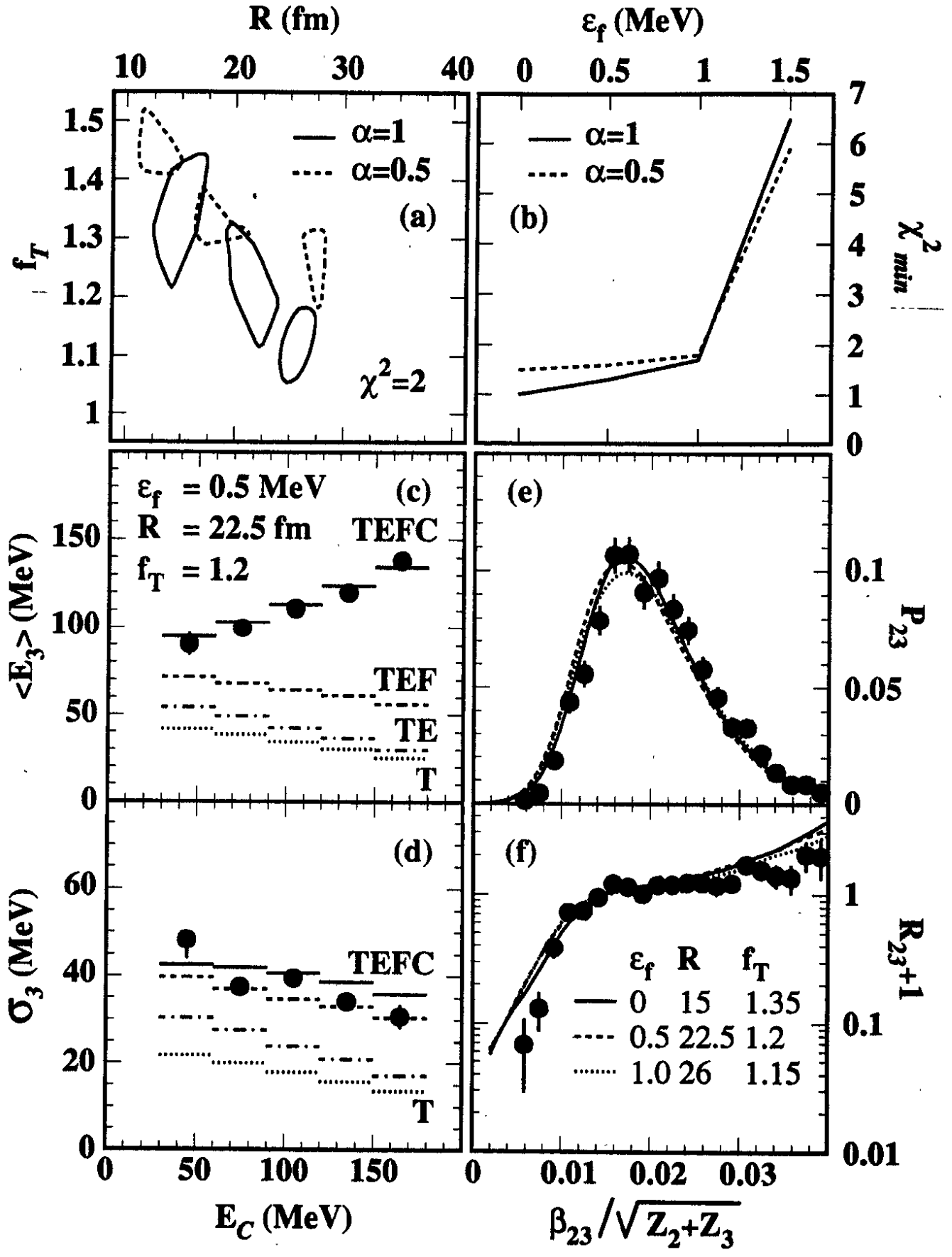
R (fm)
10
20
30
40
ε_f (MeV)
0
0.5
1
1.5
f_T
1.5
1.4
1.3
1.2
1.1
1
α=1
α=0.5
(a)
χ^2=2
(b)
χ^2_{min}
7
6
5
4
3
2
1
0
ε_f = 0.5 MeV
R = 22.5 fm
f_T = 1.2
(c)
TEFC
TEF
TE
T
<E_3> (MeV)
150
100
50
0
(e)
P_{23}
0.1
0.05
0
(d)
TEFC
T
σ_3 (MeV)
60
40
20
0
(f)
ε_f R f_T
0 15 1.35
0.5 22.5 1.2
1.0 26 1.15
R_{23}+1
1
0.1
0.01
0
50
100
150
E_C (MeV)
0
0.01
0.02
0.03
$\beta_{23}/\sqrt{Z_2+Z_3}$

Figure 3: